

A Synergistic Battery-hydrogen Network for Renewable Sharing and Energy Use in Buildings and Fuel Cell Electric Vehicles

Lu Zhou^a, Yuekuan Zhou^{a,b,c,d *}

^aSustainable Energy and Environment Thrust, Function Hub, The Hong Kong University of Science and Technology (Guangzhou), Nansha, Guangzhou, 511400, Guangdong, China

^bDepartment of Mechanical and Aerospace Engineering, The Hong Kong University of Science and Technology, Clear Water Bay, Hong Kong SAR, China

^cHKUST Shenzhen-Hong Kong Collaborative Innovation Research Institute, Futian, Shenzhen

^dDivision of Emerging Interdisciplinary Areas, The Hong Kong University of Science and Technology, Clear Water Bay, Hong Kong SAR, China

ABSTRACT

The interaction between H₂ and electricity systems increases system energy flexibility and renewable penetration with mitigation on the grid power pressure, where the hydrogen-fuel-cell vehicle is the key component during the interaction process. However, the low energy efficiency of the electricity-H₂-electricity conversion will cause massive energy loss, thus leading to an increase in operational costs and equivalent CO₂ emission (ECE). This study aims to develop systems with different degrees of synergistic collaboration between battery and hydrogen energy systems by applying three hierarchical control strategies, to investigate the impact of the hydrogen-based building-vehicle network on the operational costs of the whole community and HV owners, and ECE of the whole energy network. In addition, the system also considers a variety of renewable sources, low-grade heat recovery from electricity-to-H₂ and H₂-to-electricity conversions, the degradation of fuel cell (FC), and multi-stage grid electricity price. Results indicate that compared to the reference case without V2B/B2V, the annual total operational costs of Case 1 (V2B/B2V interaction with first charging/discharging priority given to electric battery) and Case 2 (V2B/B2V interaction first charging/discharging priority given to FCEVs) increase by 2.35% and 17.43%, but the operational costs of HV owners are reduced by 6.76% and 36.19%, respectively. Research results can provide frontier guidelines on development of synergistic battery-hydrogen network for renewable sharing and energy use in buildings and fuel cell electric vehicles.

Keywords: hydrogen vehicle, hydrogen-based interactive energy networks, equivalent CO₂ emission, energy trading, distributed hydrogen infrastructure, hydrogen economy¹

NONMENCLATURE

<i>Abbreviations</i>	
HV	Hydrogen-fuel-cell vehicle
PV	Photovoltaic
AHU	Air handling unit
V2B	Vehicle-to-building
B2V	Building-to-vehicle
DHW	Domestic hot water
FC	Fuel cell
ECE	Equivalent CO ₂ emission
Bat first	The charging and discharging of the battery take priority over the H ₂ system
H ₂ first	The charging and discharging of the H ₂ system take priority over the battery
RSR	Renewable shifted ratio

1. INTRODUCTION

Hydrogen, as one of the ideal clean energies for storage and supply with the by-product of water only, has been gradually applied in multi-energy systems for decarbonization. Due to the intermittence of renewable energy (like solar PV, wind turbine, ocean energy), energy storages are critical to improve renewable penetration and energy flexibility from buildings to power grid with mitigation on grid power pressure [1]. In addition, due to the combined heat and power production, the integration of hydrogen vehicles (HVs) with buildings can achieve mutual win-win benefits in terms of the reduction of the building DHW load, profits from building for HVs' owners, etc.

In academia, researchers focused on energy integration of electric vehicles (EVs) or fuel cell electric vehicles (FCEVs) with building energy systems. Zhou and

Cao [2] investigated the energy flexibility enhancement of the sophisticated building energy systems integrated with electric vehicles by implementing two dynamic advanced grid-responsive energy control strategies, and also discussed the techno-economic feasibility regarding different off-peak electricity tariffs and different rated renewable capacities. The authors found that the maximum of 96.8% of the grid electricity can be shifted from the off-peak period to the peak period for the usage of the office building when applying the energy shifting from grid to battery and electric vehicles in off-peak period. The comparison between hydrogen vehicles and electric vehicles is also adopted in achieving annual net-zero energy balance [3], the results showed that the system with the EV will be easier to reach the annual net-zero energy balance than the HV because of the energy efficiency of different energy storage systems. Cao and Alanne [4] comparatively conducted the techno-economic analysis between 16 groups with respect to the equipment options of the renewable resources collectors, the ground source heat pump (GSHP), and the HV refueling methods.

However, due to the low energy efficiency of H₂ conversion in electricity-H₂-electricity compared to electric battery, the energy loss of the system will increase when there is an interaction between HVs and buildings (V2B and B2V), resulting in an increase in the total operational costs and equivalent CO₂ emission (ECE) of the whole energy system.

Considering the intermittence and fluctuation of renewable energy, energy management strategies have been explored through demand-side management [5] and thermal/electrical energy storages [4]. Due to the simplification and easy implementation characteristics, most studies focused on rule-based strategies. Cao [3], Cao and Alanne [4] proposed strategies integrating buildings with hydrogen vehicle (HV) considering the transportation and the heat recovery but without the consideration about the fuel cell degradation and the cabin thermal loss of FC. In addition, the cross-disciplinary artificial intelligence has also been applied in multi-energy systems for dynamic prediction. Fonseca and Nguyen [6] described a computational framework for the analysis and optimization of energy systems in neighborhoods and city districts by presenting the City Energy Analyst (an integrated framework), and Zhou and Cao [7] implemented with an advanced multi-objective optimization algorithm (called Pareto archive NSGA-II) for optimal design and robust operation in a system integrated with buildings, vehicles, and renewables. In respect to hybrid electrical storages, i.e., hydrogen fuel cell and electrochemical battery, considering the difference of energy storage characteristics between

hydrogen fuel cell and electrochemical battery (e.g., fast charging/discharging response, low energy storage density and high energy storage efficiency of electrochemical battery, high energy storage density, idling power operation limit and low energy storage efficiency of hydrogen energy storage), there are few studies focusing on the development of collaborative operation strategies between fuel cell and electrochemical battery, to increase the intermittent renewable penetration and demand coverage.

According to differences of energy storage characteristics between hydrogen fuel cell and electrochemical battery, this study aims to develop an advanced hierarchical control strategy to achieve synergistic collaborations between battery and hydrogen energy systems for techno-economic-environmental performance improvement. A battery-hydrogen network was formulated for renewable sharing and energy use in buildings and fuel cell electric vehicles. Dynamic fuel cell degradation under idling power condition was quantified, and low-grade heat recovery from electricity-to-H₂/H₂-to-electricity conversion processes was designed for overall efficiency improvement. Furthermore, the local multi-stage grid electricity price was fully utilized in the hierarchical control strategy, for low-price grid power shifting through the synergistic battery-hydrogen storages.

2. METHODOLOGY

2.1 Scenario

The building studied in this paper is located in Guangzhou, Guangdong Province, China (23.13 °N, 113.27 °E). Both the daily and monthly associated solar radiation and the wind speeds are shown in Fig. 1. The daily solar radiation fluctuates between 0.28 and 7.54 kWh/m², and the daily average wind speed fluctuates between 0.32 and 6.16 m/s. From the monthly perspective, the monthly average solar radiation on the horizontal surface fluctuates between 62.67 and 167.9 kWh/m²-month, and the monthly average wind speed fluctuates between 2.1 and 2.6 m/s. The weather data is from Meteonorm [8]. The data of wind speed in Nansha District is collected from SCADA [9].

To increase the output of renewable energy, the wind turbines in the system are set up on Longxue island in Nansha District, Guangzhou, Guangdong, China. The daily average wind speed fluctuates between 0.34 and 14.26 m/s, and the monthly average wind speed fluctuates between 3.2 and 7.48 m/s. The comparison between typical wind speed of LongXue Island and Guangdong, as shown in Fig. 2, indicates that both the

minimum and maximum values of monthly average wind speed are much larger in LongXue Island.

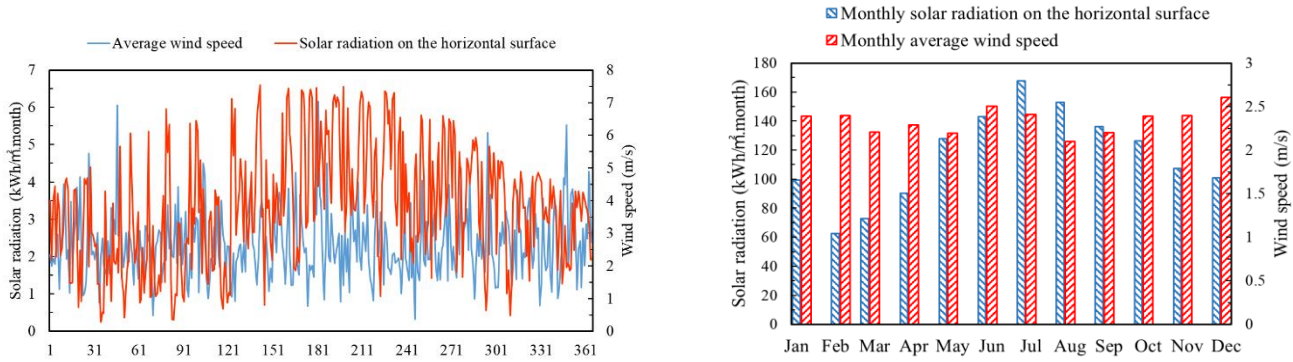


Fig. 1. Daily and monthly solar radiation and average wind speed.

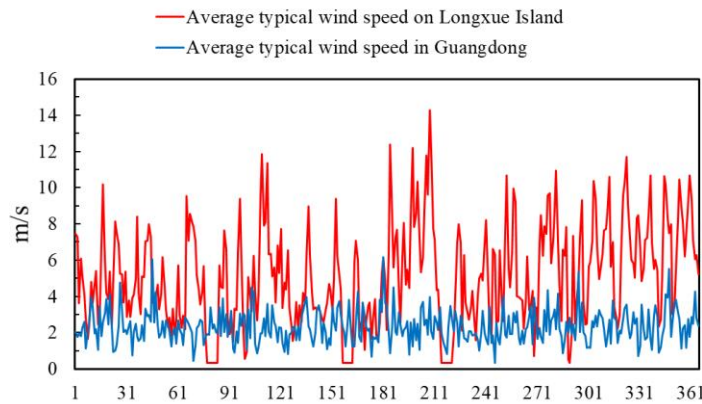


Fig. 2. Daily average wind speed on Longxue Island and typical of Guangdong.

2.2 Building information

There are three 30-floor office buildings with a net floor area of 600 m² (30m×20 m) and a height of 3 m for each floor. The window to wall ratio is 20%. Besides, both space cooling and space heating are designed to achieve indoor thermal comfort. Specific design parameters of the office building are listed in Table 1 (as shown in attachment). Considering the cogenerated heat from fuel cells, a two-stage waste heat recovery system was designed to partially cover DHW load.

Duration curves and energy loads are demonstrated in Fig. 3. Compared to the space or AHU heating load, the space or AHU cooling load is relatively higher.

The annual energy load and peak power are listed in Table 2 (as shown in attachment), including space cooling, AHU cooling, total heating (sum of space heating and AHU heating), and DHW heating. Since Guangdong has a subtropical monsoon climate that is warm in winter and hot in summer, the annual total heating is 0.21 kWh/m²·a with a peak power of 644.90 kW. The annual electric demand (including the lighting, the equipment, ventilation fans, and pumps) is 56.96 kWh/m²·a with the peak power at 357.76 kW.

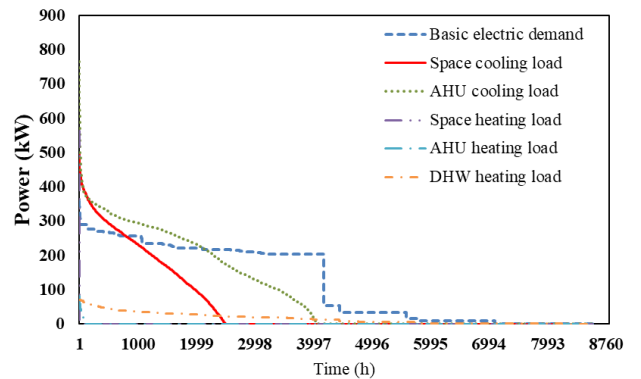


Fig. 3. Duration curves of the basic electric demand of each office building

2.3 Renewable energy systems

In order to make full use of renewable resources in Guangdong, onsite distributed renewable systems are designed in buildings, including vertical BIPVs, micro-wind turbines, and titled rooftop PVs. The BIPVs are equipped on all four facades to provide solar shading at daytime and generate renewable power,

simultaneously. Rooftop PVs are designed with tilted angle and azimuth angles of 18° and 0°, respectively. Furthermore, due to the abundance in wind energy resources in Nanshan, Guangzhou, three wind turbines with a rated capacity of 0.5 MW are installed with a hub height of 60 m. Designed parameters of the PV, BIPV, and wind turbine are listed in Table 3 (as shown in attachment), and the annual generation power of the renewable sources are listed in Table 4 (as shown in attachment).

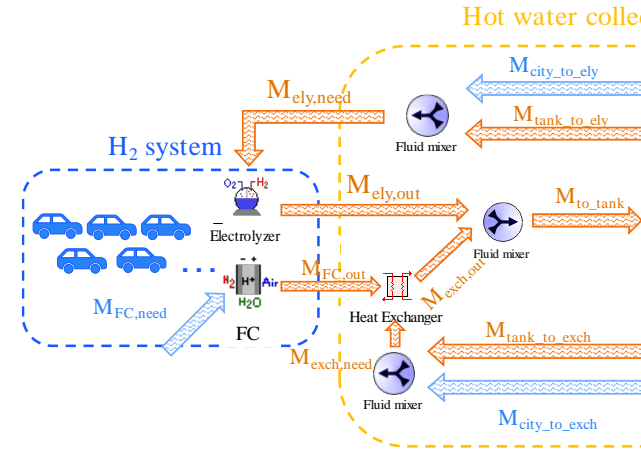
2.4 Hydrogen systems

In order to mitigate the intermittence of renewable power supply and improve its penetration, FCEVs with hydrogen are dynamically interacted with building energy systems. Electrolyzer converts surplus renewable electricity into H₂, which will be compressed and stored in a H₂ storage tank. The fuel cell in FCEVs will convert H₂ into electricity to power the daily transportation demand and support the electrical demands of the building through V2B interactions. Detailed parameters of H₂ system are listed in Table 5 (as shown in attachment).

2.5 Waste heat recovery from the hydrogen system

As most of energy is thermal energy during the gas-power conversions, the waste heat recovery can effectively improve the energy efficiency [10].

Fig. 4 shows the process of low-grade heat recovery from the H₂ system to decrease the DHW heating load of buildings. Specifically, a hot water storage tank (HWST) is designed for the simultaneous waste heat recovery from the gas-power conversions and hot water supply to buildings. Cooling water will directly extract heat from electrolyzer through a direct heat exchanger and then go into the HWST for thermal energy storage. Similarly, cooling water will extract heat from fuel cell through an indirect heat exchanger. Table 6 (as shown in attachment) lists the parameters of the waste heat recovery system.



Recovery and storage side

Fig. 4. The process of recovering the heat of

Fig. 4 shows the water flows (m³/h) during the waste heat recovery process. On the recovery and storage side, M_{ely,need} is the water required for cooling the electrolyzer and M_{ely,out} is the outlet water after the direct heat exchange. Similarly, M_{FC,need} is the mass flow rate of required coolant for FC, and the liquid outlet the FC (M_{FC,out}) will exchange heat with cooling water (M_{exch,need}) in the indirect heat exchanger to extract the heat. M_{to_tank} is the mixture of the two heat exchange flows and will enter into the water storage tank when the temperature is higher than the water in the bottom of the tank.

As the outlet water of the tank, the M_{tank_to_ely} and M_{tank_to_exch} are used as the cooling water of the electrolyzer and heat exchanger to avoid heat waste, and they will be mixed with city water (M_{city_to_ely} and M_{city_to_exch}) if the tank outlet water is not sufficient for cooling. For the end-user side, city water will enter the diverter and then separately enter the water tank (M_{city_to_tank}) and fluid mixer (M_{city_to_mixer}) to ensure the temperature of mixed water from the water tank (M_{tank,out}) and the city water (M_{city_to_mixer}) to the electric heater (M_{mixer}) is closest to the required temperature.

Finally, the hot water from the mixer will be heated by the auxiliary electric heater to guarantee the supplied hot water temperature (60 °C).

To keep the water in the tank stable and meet the needs of domestic hot water, mass balance of water flows needs to be followed, as shown below.

$$M_{to_tank} = M_{tank_to_ely} + M_{tank_to_exch} \quad (1)$$

$$M_{city_to_tank} = M_{tank,out} \quad (2)$$

$$M_{city} = M_{DHW,need} \quad (3)$$

higher than L_e , the surplus renewable energy ($P_{REe,surp1} = P_{REe} - L_e$) firstly charges battery (when $FSOC_{battery} < 0.95$), before being absorbed by the H₂ system ($P_{REe,surp2}$). Afterwards, if $P_{REe,surp2}$ is lower than the sum of the idling

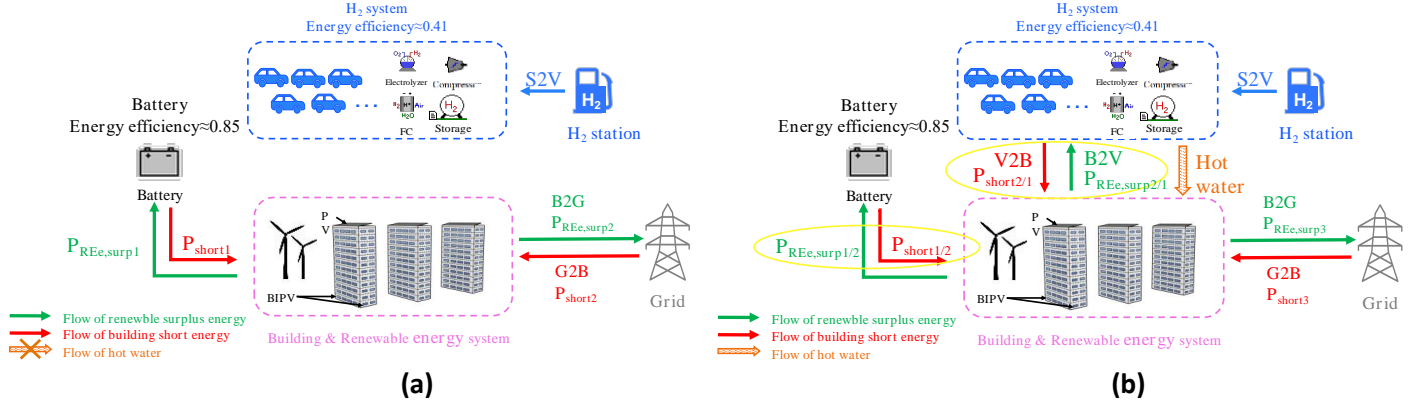


Fig. 5. Synergistic battery-hydrogen networks for renewable sharing and energy use in buildings and fuel cell electric vehicles in (a) reference case (isolated system without V2B/B2V interactions); (b) Case 1 (first charging/discharging priority on battery), Case 2 (first charging/discharging priority on H₂ systems).

2.6 Energy management and control strategy

Fig. 5 shows the synergistic battery-hydrogen energy network for renewable sharing and energy use in buildings and fuel cell electric vehicles. The energy network is consisted of buildings, battery, power grid, and fuel cell electric vehicles (FCEVs). The surplus renewable energy from solar PVs is shared by both buildings and FCEVs to decarbonize the integrated energy system with high renewable penetration. Depending on whether there is an interaction between hydrogen vehicles and buildings and charging/discharging priority of the H₂ system, three cases are formulated in this study, i.e., reference case (without V2B/B2V interactions), Case 1 (battery charging/discharging first) and Case 2 (H₂ charging/discharging first). Dynamic power flow of three cases is demonstrated in Fig. 6.

Reference case (without V2B/B2V interactions): as shown in Fig. 6. (a), energy interaction can be realized between the static battery, buildings, and the power grid. H₂ is only used as the fuel of HVs to meet daily transportation. If onsite solar power (P_{REe}) is higher than building demand (L_e), the surplus energy ($P_{REe,surp1} = P_{REe} - L_e$) is used to charge the battery before being exported to the grid when the $FSOC_{battery}$ is lower than 0.95. If the P_{REe} is less than L_e and $FSOC_{battery}$ is higher than 0.3, the demand shortage ($P_{short1} = L_e - P_{REe}$) is firstly covered by the energy discharged from the battery before importing from the grid.

Case 1 (Battery charging/discharging first): as shown in Fig. 6. (b), if there is a surplus renewable energy/demand shortage, battery will be given the first priority for charging/discharging. To be specific, If P_{REe} is

power ($P_{ely,idling}$) of the electrolyzer and the compressor power (P_{comp}), or the H₂ tank is fully charged ($SOC_{upper,limit} = 0.95$), the $P_{REe,surp2}$ will be directly delivered to the grid. Otherwise, the $P_{REe,surp2}$ will be delivered to the H₂ system for producing H₂ gas. On the other hand, if the P_{REe} is less than L_e , the demand shortage ($P_{short1} = L_e - P_{REe}$) will firstly be covered by battery (when $FSOC_{battery} > 0.3$). Next, the demand shortage (P_{short2}) will be covered by power discharging from FCEVs ($P_{H2,dischar}$) if the H₂ tank is not fully discharged ($SOC_{lower,limit} \geq 0.11$), and P_{short2} is higher than the PEMFCs' idling power ($P_{FC,idling}$). Finally, the rest demand shortage (P_{short3}) will be covered by energy imported from the local grid. Otherwise, P_{short2} is directly covered by the electricity imported from the local grid.

Case 2 (H₂ charging/discharging first): contrary to the Case 1, the first charging/discharging priority is given to H₂ systems, followed by battery. The justification of the strategy is to penetrate renewable energy as much as possible in transportation and utilize H₂ energy for energy decarbonization.

In three cases, the vehicles' FC converts H₂ into power through the gas-to-power conversion process, to fully cover energy consumption for daily transportation and partially cover energy demands in buildings through the V2B interaction. Furthermore, in order to address the cruise anxiety, the HVs will be charged into the threshold state ($SOC_{V2B,thres}$) half an hour before the daily transportation in the H₂ station.

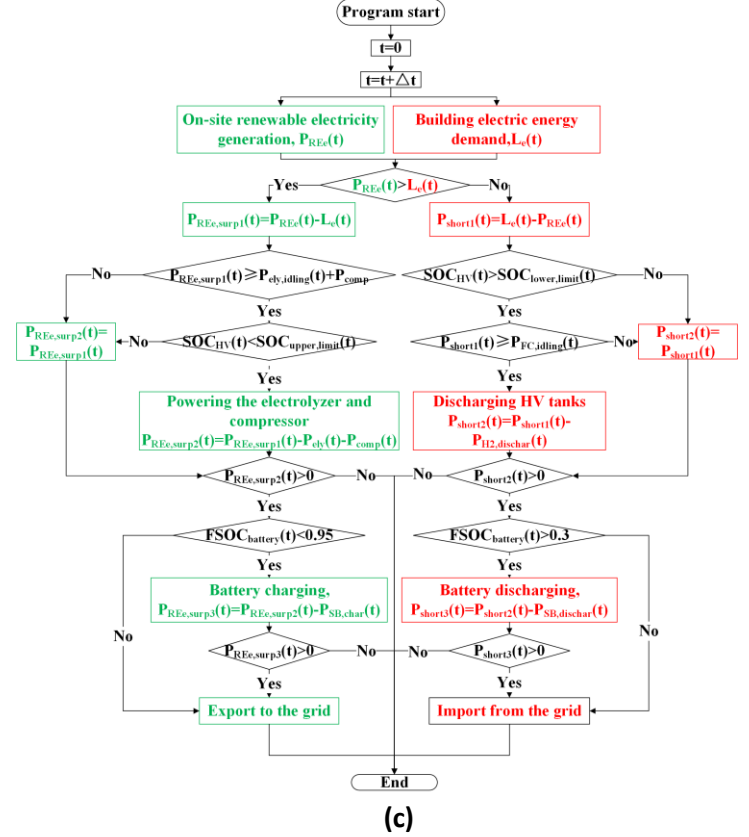
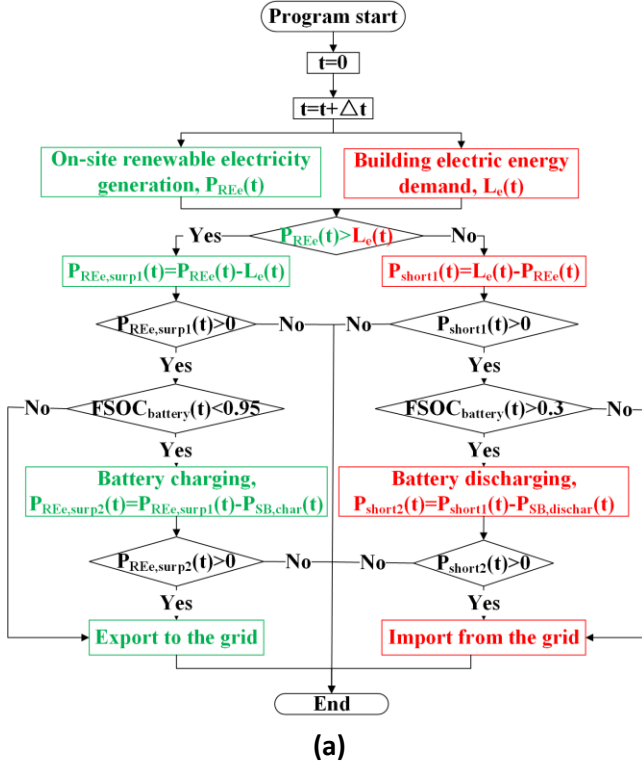


Fig. 6 Dynamic power flow for **(a)** reference case (No V2B/B2V interactions); **(b)** Case 1 (first charging/discharging priority for battery system). **(c)** Case 2 (first charging/discharging priority for H₂ system)

2.7 System assessment criteria

2.7.1 Energy flexibility investigation

To quantify the energy flexibility of the hybrid energy systems with diversified energy storage systems, the off-peak surplus renewable shifted ratio (RSR) is introduced. RSR is the proportion of renewable energy stored during off-peak period ($E_{\text{off-peak,REE,stored}}$) to the total on-site surplus renewable energy ($E_{\text{surp,REE}}$).

$$E_{\text{off-peak,REE,stored}} = \int_0^{t_{\text{off-peak}}} [P_{\text{toSB,REE}}(t) + P_{\text{toEly,REE}}(t)] dt \quad (4)$$

$$E_{\text{surp,REE}} = \int_0^{t_{\text{end}}} P_{\text{surp,REE}}(t) dt \quad (5)$$

$$\text{RSR} = \frac{E_{\text{off-peak,REE,stored}}}{E_{\text{surp,REE}}} \quad (6)$$

2.7.2 Economic performance

To investigate the impact of different hierarchical control strategies on the cost of the system regarding the interface between the hybrid building–vehicle system and the electricity grid, the annual total operational costs of the integrated energy network (C_{total}) and the operational costs of HV owners (C_{HV}) are calculated (as shown in Eq. (14) and Eq. (13)). C_{total} includes three parts, the cost of electricity from grid (C_e), H₂ delivered from

pipeline (C_{H_2}), and equivalent cost of fuel cell degradation ($C_{degradation}$).

With respect to HV owners, C_{HV} includes C_{H_2} , $C_{degradation}$, and economic benefits obtained from buildings by participating in V2B interactions. Mathematical equations are listed below:

$$IC = \int_0^{end} [P_{imp, extreme-peak}(t) \cdot C_{grid, import, extreme-peak} + P_{imp, peak}(t) \cdot C_{grid, import, peak} + P_{imp, flat}(t) \cdot C_{grid, import, flat} + P_{imp, off-peak}(t) \cdot C_{grid, import, off-peak}] dt \quad (7)$$

$$EC = \int_0^{end} [P_{exp}(t) \cdot C_{grid, feed-in-tariff}] dt \quad (8)$$

$$C_e = IC - EC \quad (9)$$

$$C_{H_2} = \int_0^{end} [M_{H_2, station}(t) \cdot C_{H_2, station}] dt \quad (10)$$

$$C_{degradation} = D_{FC} \cdot n_{FC} \cdot 3685 \quad (11)$$

$$C_{gain \text{ from building}} = \int_0^{end} [P_{HV-to-building}(t) \cdot C_{HV-to-building}(t)] dt \quad (12)$$

$$C_{HV} = C_{H_2} + C_{degradation} - C_{gain \text{ from building}} \quad (13)$$

$$C_{total} = C_e + C_{H_2} + C_{degradation} \quad (14)$$

where IC is the electricity import cost, $P_{imp, extreme-peak}(t)$, $P_{imp, peak}(t)$, $P_{imp, flat}(t)$, $P_{imp, off-peak}(t)$ are the power imported from the grid during extreme peak, peak, flat, and off-peak periods (kW) at timestep t , respectively. $C_{grid, import, extreme-peak}$, $C_{grid, import, peak}$, $C_{grid, import, flat}$ and $C_{grid, import, off-peak}$ refer to the price of electricity imported from the grid during different periods (CNY/kWh). Table 7 (as shown in attachment) shows the multi-stage grid electricity price in Guangzhou. According to the announcement issued by China Southern Power Grid in April 2022 [11]. For commercial buildings, the electricity price is divided into four periods (peak (10:00pm-12:00pm, 14:00pm-19:00pm), flat (08:00am-10:00pm, 12:00pm-14:00pm, 19:00pm-24:00pm), and off-peak (00:00am-08:00am) period). Besides, In July, August and September, or days when the maximum temperature exceeds 35 °C, the time during 11:00am-12:00pm and 15:00pm-17:00pm is defined as the extreme-peak period. For the commercial building with an electric voltage lower than 1000V, the price of electricity in the extreme-peak, peak, flat, off-peak periods are 1.7361, 1.3944, 0.8316, 0.3332 CNY/ kWh, respectively. The $P_{exp}(t)$ refers to the power exported to the grid at the simulation time t , and $C_{grid, feed-in-tariff}$ refers to the grid

feed-in tariff, which is the same as the local benchmark price of coal-fired power generation in Guangzhou, Guangdong (0.453 CNY/kWh) according to the electricity price policy issued by the national development and Reform Commission in 2021 [12]. C_{H_2} refers to the cost of hydrogen from H_2 station during mandatory charging period. According to the transaction price in Guangdong, the price of hydrogen imported from H_2 station ($C_{H_2, station}$) is about 30 CNY/kg [13]. $C_{degradation}$ is the annual degradation cost of HV, and the D_{FC} is the ratio of the annual fuel cell degradation of each vehicle. The n_{FC} is the number of vehicles, and 3685 is the equivalent cost of degradation (3685 CNY for 1% performance degradation in fuel cells [14]) [15]. $C_{gain \text{ from building}}$ is the economic earning from buildings to vehicles by participating in the V2B. In this simulation, the study assumes that the buy-in cost of building owners is the same between HV owners and power grid.

2.7.3 Equivalent CO₂ emission

For the hybrid building–vehicle system, the annual net equivalent CO₂ emission, ECE_a is introduced to quantitatively investigated the impact of the building's energy consumption on the environment. The mathematical equation is shown in Eq. (16).

$$P_{equivalent, H_2, station}(t) = EEF_{H_2} \cdot M_{H_2, station}(t) \quad (15)$$

$$ECE_a = \int_0^{end} \left(\begin{array}{l} P_{imp, building}(t) \cdot CEF_{eg} \\ -P_{exp, building}(t) \cdot CEF_{eg} \\ + P_{equivalent, H_2, station}(t) \cdot CEF_{eg} \end{array} \right) dt \quad (16)$$

where CEF_{eg} is the equivalent CO₂ emission factor of the electricity grid. The territory-wide default value of CEF_{eg} is 0.6379 kg CO_{2,eq}/ kWh_{end} according to the literature [16]. $EEF_{H_2}(t)$ is the equivalent electricity of H_2 imported from H_2 station, 48.7kWh/kg, which is the average power required for electrolyzer to produce 1kg H_2 in the annual simulation. $M_{H_2, station}(t)$ (kg) is the H_2 imported from H_2 station in mandatory charging process of HVs.

Furthermore, it is assumed that the equivalent CO₂ emission factor of the renewable electricity generated on-site from the PV, BIPV, and wind turbine is 0 according to the [16].

3. RESULTS AND DISCUSSIONS

3.1 Impact of different control strategies on energy flexibility

As shown in Fig. 7, the cases with the interaction between H_2 system and buildings have higher off-peak surplus renewable shifted ratio than not, and Case 2 (with first charging/discharging priority for H_2 system) has the highest RSR among the three cases.

In Case 1 and Case2, the RSR increase 7.8% and 15.2% compared to the reference case, from 30% to 32.37% and 34.58%, respectively. This is because that, compared to reference case with single electricity storage system, the on-site surplus renewable energy can be more stored by the hybrid electricity storage systems during the off-peak period. Moreover, in Case 1 and Case 2, for the different charging/discharging priorities for H₂ system, the energy flows into the H₂ system in Case 1 is more limited by the idling power of electrolyzer and the upper limit of the H₂ tank. The reason is that, in Case 1, sometimes there is just little energy left for the hydrogen system absorption or hydrogen in the tank is blocked in the tank due to the low utilization rate of H₂ energy.

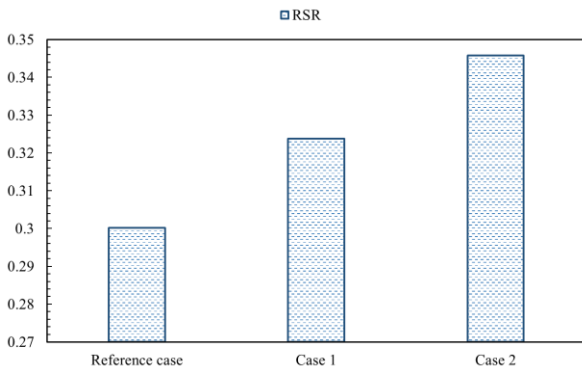
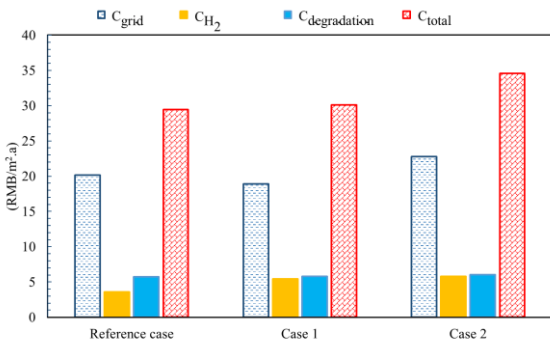


Fig. 7. The penetration level of renewable energy in three cases

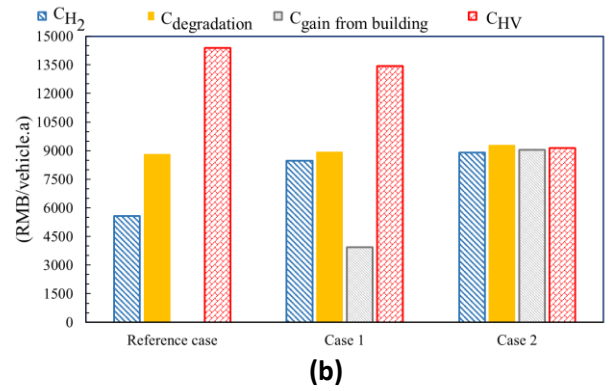
(**Note:** reference case refers to the case without V2B/B2V; Case 1 refers to battery charging/discharging first; Case 2 refers to H₂ charging/discharging first. More details can be checked in Section 2.6)

3.2 Comparative analysis on economic performance between electrochemical battery and hydrogen

Table 8 (as shown in attachment) compares the annual energy efficiency and energy loss of H₂ system, battery, and the whole energy network. Due to the low power efficiency of H₂ during power-to-gas-to-power conversion, the system with higher utilization of H₂ energy leads to lower energy efficiency and higher energy loss.



(a)



(b)

Fig. 8 (a) annual operational costs; **(b)** annual operational costs of the HV owners

Fig. 8 (a) shows the annual operational costs for the whole energy system, Fig. 8 (b) shows the annual operational costs of the HV owners (CNY/vehicle·a). The annual operational costs for the whole energy system is increased when there is the integration with H₂ system or H₂ system takes priority over the battery. However, the costs of HV owners decreased in cases with integrated H₂ system and reach minimum in Case 2 at 9142.62 CNY/vehicle·a.

To be specific, for the whole energy system, compared to the reference case, since there is interaction between H₂ system and buildings in the Case 1, the grid import cost (C_e) is reduced due to the large penetration level of renewable energy in hybrid energy systems. However, V2B also leads to hydrogen consumed, therefore more hydrogen is imported to meet the daily transportation of HVs from the H₂ station, resulting in a higher cost of hydrogen (C_{H₂}). As a result, compared to the reference case, the total operational cost (C_{total}) is increased by about 2.35%. Furthermore, compared with the Case 1, in the Case 2, C_e, C_{H₂}, and C_{total} increase with different magnitude. The main reason is due to the first charging/discharging priority is given to hydrogen energy systems with a much lower energy conversion efficiency (as shown in Fig. 5). As a result, compared to the reference case, the total operational cost (C_{total}) of the Case 2 is increased by 17.43%.

For HV owners, although the cost of H₂ (C_{H₂}) and cost of degradation (C_{degradation}) are increased in Case 1 and Case 2 compared with reference case, the interaction between H₂ system and buildings can bring money from buildings (gain from building) during V2B for HV owners, and more H₂ participate in V2B results in more money.

As a result, the annual operating cost of HV owners (C_{H₂}) in Bat first case and H₂ first case decreased by 6.76% and 36.19% compared with reference case. So, for HV owners, the integration with buildings will greatly result in the reduction of HVs costs. They will be highly motivated if the saved cost is high.

3.3 Impact of electrochemical battery and hydrogen on equivalent CO₂ emission

Fig. 9 shows the annual ECE (ECE_a) of the three cases. It can be seen that higher priority use of hydrogen will lead to greater ECE. In Case 1 and Case 2, ECE increases by 22.71% and 56.07%, respectively, compared with the reference case, since more H₂ participating in the energy flow process will lead to greater energy loss, resulting in higher ECE.

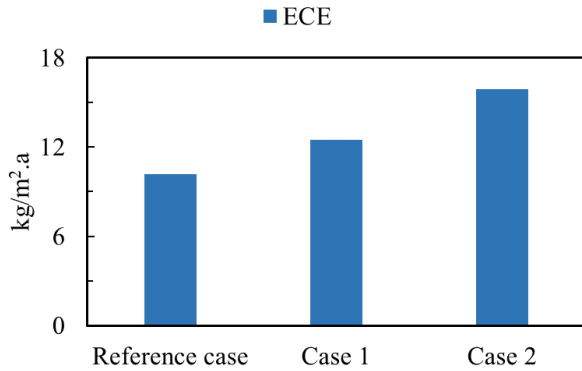


Fig. 9. The annual ECE of the whole community (ECE_a)

4. CONCLUSIONS

As one of the critical mediums for cascade energy utilization, hydrogen will play critical roles in district energy system decarbonisation. Furthermore, the hydrogen-power fuel cell electric vehicles (FCEVs) show great potentials in long-distance cruise, high energy density, and no pollution with by-products of water only. The energy interaction between renewable-powered buildings and FCEVs can mitigate the impact of renewable intermittence and decarbonize the transportation. However, due to different energy storage characteristics between hydrogen fuel cell and electrochemical battery, the integration of HV will have great impacts on the techno-economic performance of the system. In this study, three cases with different collaborative operation strategies between fuel cell and electrochemical battery are discussed, considering real-time difference between hydrogen and electricity prices, idling power and degradation of hydrogen-associated equipment, and the waste heat recovery from gas-power conversion. Main conclusions are summarised as follows:

(1). For the cases with building-vehicle integrations, the total operational costs of the system increase due to the lower energy efficiency of H₂ and the higher use of H₂ as an energy carrier will lead to higher operational costs. Compared with the case without interactions between H₂ systems and the building, the energy interaction between buildings, electric batteries and fuel cell electric vehicles will increase the annual operational cost by 2.35% and 17.43% for Case 1 (first charging/discharging

priority given to electric battery) and Case 2 (first charging/discharging priority given to FCEVs), respectively.

(2). By participating in V2B interactions, HV owners can be economically incentivized with the decrease in annual operational costs of vehicles. The research results indicate that the Case 1 (first charging/discharging priority given to electric battery) and Case 2 (first charging/discharging priority given to FCEVs), the operational costs of HV are reduced by 6.76% (from 14327.52 to 13359.68 CNY/vehicle-a) and 36.19% (from 14327.52 to 9142.62 CNY/vehicle-a), respectively.

(3). The equivalent CO₂ emission (ECE) of the integrated multi-energy system will be increased due to the low energy storage efficiency. Compared to the reference case without V2B/B2V interactions, the Case 1 and Case 2 will increase the ECE by 22.71% (from 10.19 to 12.50) and 56.07% (from 10.19 to 15.9).

ACKNOWLEDGEMENT

This work was supported by the Hong Kong University of Science and Technology (Guangzhou) startup grant (G0101000059).

ATTACHMENT

Table 1. Key parameters of the buildings.

Occupant density	10 m ² /person [17]
Infiltration rate	0.288
Maximum heat gain from the equipment	9 W/m ²
Maximum heat gain from the lighting	9 W/m ²
Maximum heat gain from each person	126W
Mass flow rate of supply air	36.12 kg/person·h [17]
Setpoint temperature for ventilation	17–21 °C
Indoor air setpoint temperature	21 °C/26 °C when the heating/cooling system is on [17]
Rated capacity and COP of the AHU cooling chiller	857.9 kW/2.92 (RTAC 240 High Efficiency [18])
Rated capacity and COP of the space cooling chiller	506 kW/2.8 (Carrier 30RB522 [19])
Specific daily hot water consumption	0.36 m ³ /(floor·day) [20]
Setpoint temperature of hot water	60 °C [20]

Table 2. Annual energy load and peak power

Space cooling load (kWh/m ² ·a)/Peak power (kW)	27.58/499.36
AHU cooling load(kWh/m ² ·a)/Peak power (kW)	48.18/764.76

Total heating load (kWh/m ² ·a)/Peak power (kW)	0.21/644.90
DHW energy demand(kWh/m ² ·a)/Peak power (kW)	7.80/69.90
Basic electric demand (kWh/m ² ·a)/Peak power (kW)	56.96/357.76
Total electric demand (kWh/m ² ·a)/Peak power (kW)	95.92/893.78

Table 3. The designed parameters of the renewable system.

Component	Parameter	Value
PV panels	Type in TRNSYS 18	567
	Collector length (m)	20
	Collector width (m)	2
	Channel height (m)	0.1
	Reference PV efficiency	0.22
	Temperature coefficient (/°C)	-0.003
	Number of modules	600
	Area of each module(m ²)	0.89 m ²
BIPV	The type used in TRNSYS 18	567
	Total area for the community (m ²)	17964
	Efficiency under standard testing conditions (25 °C and 1000 W/m ²)	14.27%
	Cover Emissivity	0.9
	Cover Conductivity	5.04
	Cover Thickness	0.00635
	Substrate Resistance	0.422
	Channel Emissivity - Top	0.09
	Channel Emissivity - Bottom	0.9
	Back Resistance	0.1204
	Channel Height	0.0508
	The absorptance of the surface for solar radiation	0.9
	Refractive Index	1.526
	Extinction Coefficient (m ⁻¹)	4
	Reference PV Efficiency	0.1427
	Reference Temperature	25
	Reference Radiation(W/m ²)	1000
	Efficiency Modifier	-0.005
	Efficiency Modifier – Radiation (m ² /W)	0.00009
	Wind turbine	The type used in TRNSYS 18
The type of the wind turbine		3-blade horizontal-axis wind turbine (based on the commercial product)
	Hub height (m)	60

Rotor diameter (m)	44
Rated wind speed (m/s)	10
Cut-in wind speed (m/s)	3.5
Cut-out wind speed (m/s)	25
The site shear exponent	0.22
Rated power for one wind turbine (MW)	0.5

Table 4. Annual renewable energy and peak power of renewable energy sources.

	Generation power
Rooftop PV (kWh/m ² ·a)/Peak power (kW)	4.60/59.71
Wind turbine (kWh/m ² ·a)/Peak power (kW)	68.26/500
BIPV (kWh/m ² ·a)/Peak power (kW)	23.61/276.27

Table 5. Detailed parameters of H2 system.

Component	Parameter	Value
Electrolyzer	Type in TRNSYS 18	160a
	Electrode area (m ²)	0.5
	Number of cells per stack	50
	Number of stacks	5
	Cooling water inlet temperature (°C)	Case-dependent
	Cooling water flow rate (m ³ /h)	1
	Operating temperature (°C)	80
Compressor	Type in TRNSYS 18	167
	Number of parallel compressors	1
	Number of compressor stages	3
	Desired pressure (bar)	700
H ₂ storage tank (for 35 HVs)	Type in TRNSYS 18	164b
	Maximum pressure (bar)	700
	Tank volume (m ³)	4.27
FC	Type in TRNSYS 18	170a
	Number of cells per stack	100
	Number of stacks	25
	Electrode area (cm ²)	8000
	Coolant inlet temperature (°C)	20
	Coolant temperature rise (°C)	30

Table 6. Parameters of heat recovery system.

Domestic tankless heater	Type in TRNSYS 18	138
	Maximum heating rate (kW)	80
	Set-point temperature (°C)	60

Heat exchanger	Type in TRNSYS 18	5
	Load side inlet temperature (°C)	Case-dependent
	Overall heat transfer coefficient (W/ K)	7200
Water tank	Type in TRNSYS 18	39
	Overall tank volume (m ³)	20
	Tank height(m)	4
	Top loss coefficient (kJ/h·m ² ·K)	1.08
	Edge loss coefficient (kJ/h·m ² ·K)	1.08
	Bottom loss coefficient (kJ/h·m ² ·K)	1.08

Table 7. Multi-stage grid electricity price in Guangdong.

Specific import costs of the office building in Guangzhou

U _{ele}	C _{grid,import} (CNY/kWh)				C _{grid,feed-in tariff} (CNY/kWh)
	Extreme-peak period	Peak period	Flat period	off-peak period	
U _{ele} <1000V	1.7361	1.3944	0.8316	0.3332	0.453

Table 8. Energy loss and energy efficiency of H₂ system, battery, and the whole energy network

	Energy loss in HV system (kWh)	Energy loss in HV system (kWh)	Energy efficiency of H ₂ system	Energy loss in Battery	Energy loss in whole system (kWh)	Overall efficiency
	without heat recovery	with heat recovery	with heat recovery			
Reference Case	185326.26	185326.26	0.41	23613.258	762562.2	0.89
Case 1	382558.98	370990.95	0.43	23620.842	969996.95	0.86
Case 2	788192.03	747015.37	0.44	16094.695	1287216.34	0.82

(Note: considering heat recovery means that the heat used for covering DHW load during the operation of H₂ system is regarded as the energy generation of H₂ system).

REFERENCE

[1] Rodrigues EMG, Godina R, Santos SF, Bizuayehu AW, Contreras J, Catalão JPS. Energy storage systems supporting increased penetration of renewables in islanded systems. *Energy* 2014;75:265–80. <https://doi.org/10.1016/j.energy.2014.07.072>.

[2] Zhou Y, Cao S. Energy flexibility investigation of advanced grid-responsive energy control strategies with the static battery and electric vehicles: A case study of a high-rise office building in Hong Kong. *Energy Convers Manag* 2019;199:111888. <https://doi.org/10.1016/j.enconman.2019.111888>.

[3] Cao S. Comparison of the energy and environmental impact by integrating a H₂ vehicle and an electric vehicle into a zero-energy building. *Energy Convers Manag* 2016;123:153–73. <https://doi.org/10.1016/j.enconman.2016.06.033>.

[4] Cao S, Alanne K. The techno-economic analysis of a hybrid zero-emission building system integrated with a commercial-scale zero-emission hydrogen vehicle. *Appl Energy* 2018;211:639–61. <https://doi.org/10.1016/j.apenergy.2017.11.079>.

[5] Wu Y, Ravey A, Chrenko D, Miraoui A. Demand side energy management of EV charging stations by approximate dynamic programming. *Energy Convers Manag* 2019;196:878–90. <https://doi.org/10.1016/j.enconman.2019.06.058>.

[6] Fonseca JA, Nguyen TA, Schlueter A, Marechal F. City Energy Analyst (CEA): Integrated framework for analysis and optimization of building energy systems in neighborhoods and city districts. *Energy Build* 2016;113:202–26. <https://doi.org/10.1016/j.enbuild.2015.11.055>.

[7] Zhou Y, Cao S, Kosonen R, Hamdy M. Multi-objective optimisation of an interactive buildings-vehicles energy sharing network with high energy flexibility using the Pareto archive NSGA-II algorithm. *Energy Convers Manag* 2020;218:113017. <https://doi.org/10.1016/j.enconman.2020.113017>.

[8] Meteorm, <https://meteorm.com/>.

[9] SCADA, <https://en.wikipedia.org/wiki/SCADA>;

[10] Zhou Y. Transition towards carbon-neutral districts based on storage techniques and spatiotemporal energy sharing with electrification and hydrogenation. *Renew Sustain Energy Rev* 2022;162:112444. <https://doi.org/10.1016/j.rser.2022.112444>.

[11] China Southern Power Grid, Announcement of Guangdong Power Grid Co., Ltd. on the Price of Purchasing Electrician Commercial Users in April; 2022.

[12] National Development and Reform Commission, Notice on Issues Related to New Energy on Grid Tariff Policy, China; 2021.

[13] Bureau of Development and Reform of Nanhai District of Foshan City, Three-Year Action Plan for Promoting the Development of Hydrogen Energy Industry in Nanhai District, Foshan City, Guangdong, China (2022-2025); 2022

[14] China Foreign Exchange Trade System, average exchange rate of RMB/US dollar; 2022.04

[15] He Y, Zhou Y, Wang Z, Liu J, Liu Z, Zhang G. Quantification on fuel cell degradation and techno-economic analysis of a hydrogen-based grid-interactive residential energy sharing network with fuel-cell-powered vehicles. *Appl Energy* 2021;303:117444.

<https://doi.org/10.1016/j.apenergy.2021.117444>.

[16] Ministry of Housing and Urban-Rural Development of the People's Republic of China, Guidelines for Carbon Dioxide Emission Information Reporting of Enterprises (Units) in Guangdong Province, China; 2022.

[17] Ministry of Housing and Urban-Rural Development of the People's Republic of China, Office Building Design Standard, JGJ/T67-2019; 2020

[18] Manualzz, Trane RTAC 130, RTAC 155 Installation Operation & Maintenance.

<https://manualzz.com/doc/55215344/trane-rtac-130--rtac-155-installation-operation-and-maintenance>;

[19] Air-Cooled Liquid Chillers with Integrated Hydronic Module, 30RB 162-802 Nominal cooling capacity 162-774 kW. <https://climamarket.bg/wp-content/uploads/Tech-Spec-Carrier-30RB-162-802.pdf>;

[20] Ministry of Housing and Urban-Rural Development of the People's Republic of China, Design Standard for Building Water Supply and rainage, GB50015-2019; 2019